RNA polymerase I–specific subunits promote polymerase clustering to enhance the rRNA gene transcription cycle

Benjamin Albert,[1,2] Isabelle Léger-Silvestre,[1,2] Christophe Normand,[1,2] Martin K. Ostermaier,[1,2] Jorge Pérez-Fernández,[1,2] Kostya I. Panov,[3] Joost C.B.M. Zomerdijk,[4] Patrick Schultz,[5] and Olivier Gadal[1,2]

[1]Laboratoire de Biologie Moléculaire des Eucaryotes du Centre National de la Recherche Scientifique and [2]Université de Toulouse, F-31000 Toulouse, France
[3]Medical Biology Centre, School of Biological Sciences, The Queen's University of Belfast, Belfast BT9 7BL, Northern Ireland, UK
[4]Wellcome Trust Division for Gene Regulation and Expression, College of Life Sciences, University of Dundee, Dundee DD1 5EH, Scotland, UK
[5]Department of Integrated Structural Biology, Institut de Génétique et de Biologie Moléculaire et Cellulaire, Centre National de la Recherche Scientifique/Institut National de la Santé et de la Recherche Médicale/Strasbourg University, Illkirch 67404, France

RNA polymerase I (Pol I) produces large ribosomal RNAs (rRNAs). In this study, we show that the Rpa49 and Rpa34 Pol I subunits, which do not have counterparts in Pol II and Pol III complexes, are functionally conserved using heterospecific complementation of the human and *Schizosaccharomyces pombe* orthologues in *Saccharomyces cerevisiae*. Deletion of *RPA49* leads to the disappearance of nucleolar structure, but nucleolar assembly can be restored by decreasing ribosomal gene copy number from 190 to 25. Statistical analysis of Miller spreads in the absence of Rpa49 demonstrates a fourfold decrease in Pol I loading rate per gene and decreased contact between adjacent Pol I complexes. Therefore, the Rpa34 and Rpa49 Pol I–specific subunits are essential for nucleolar assembly and for the high polymerase loading rate associated with frequent contact between adjacent enzymes. Together our data suggest that localized rRNA production results in spatially constrained rRNA production, which is instrumental for nucleolar assembly.

Introduction

In all living organisms, multisubunit DNA-dependent RNA polymerases are built around a common set of five core subunits ($\alpha_2\beta\beta'\omega$ in eubacteria; Minakhin et al., 2001) In archeal and eukaryotic enzymes, five additional subunits (related through common ancestry) are required, leading to a 10-subunit extended core (Cramer et al., 2008; Kwapisz et al., 2008). In eukaryotes, three nuclear RNA polymerases are found, each transcribing a dedicated set of genes. RNA polymerase II (Pol II) transcribes all protein-coding genes and most of the small nuclear RNA genes. RNA polymerase III (Pol III) is transcribing 5S ribosomal RNA (rRNA) genes, tRNA genes, and some noncoding RNA genes. RNA polymerase I (Pol I) produces a single transcript, the large polycistronic precursor (35S pre-rRNA in yeast) processed in multiple successive steps into the mature rRNAs (in yeast,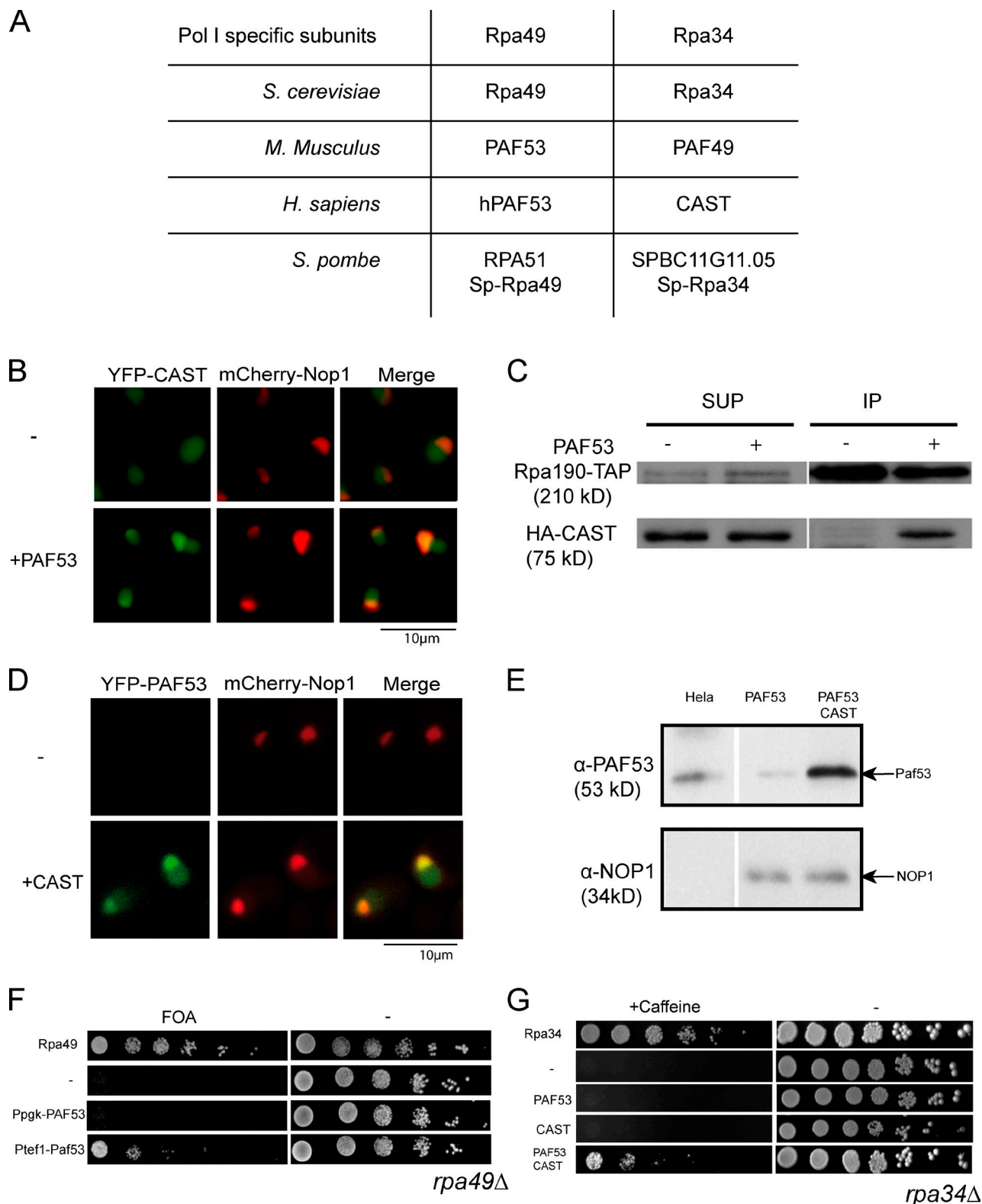 25S, 18S, and 5.8S rRNAs). Pol II is composed of 12 subunits, including a 10-subunit extended core and a peripheral heterodimer of subunits Rpb4/Rpb7. Rpb4 and Rpb7 have counterparts in Pol I and Pol III, Rpa43/Rpa14 and Rpc17/Rpc25, respectively. Pol I and Pol III have counterparts to each of the 12 Pol II subunits and, in addition, two and five specific subunits, respectively, which may be responsible for some of the specific functions of these two enzymes. In this study, we focus on Pol I–specific subunits Rpa34 and Rpa49, which have structural homology with the Rap74/Rap30 subunits of the Pol II transcription factor TFIIF (Kuhn et al., 2007).

Pol I is the most active and abundant RNA polymerase in eukaryotes. Its enormous transcriptional output can best be visualized using the DNA spread method previously developed by Miller et al. (1969), where the 35S rRNA genes (rDNA) adopt a "Christmas tree" conformation. In *Saccharomyces cerevisiae*,

Correspondence to Olivier Gadal: gadal@biotoul.fr

Abbreviations used in this paper: FOA, fluoroorotate; GIM, genetic interaction mapping; PFGE, pulse-field gel electrophoresis; rRNA, ribosomal RNA; WT, wild type.

The Rockefeller University Press $30.00
J. Cell Biol. Vol. 192 No. 2 277–293
www.jcb.org/cgi/doi/10.1083/jcb.201006040

JCB 277

A

Pol I specific subunits	Rpa49	Rpa34
S. cerevisiae	Rpa49	Rpa34
M. Musculus	PAF53	PAF49
H. sapiens	hPAF53	CAST
S. pombe	RPA51 Sp-Rpa49	SPBC11G11.05 Sp-Rpa34

B

YFP-CAST   mCherry-Nop1   Merge

−

+PAF53

10µm

C

	SUP		IP	
PAF53	−	+	−	+

PAF53
Rpa190-TAP
(210 kD)

HA-CAST
(75 kD)

D

YFP-PAF53   mCherry-Nop1   Merge

−

+CAST

10µm

E

Hela   PAF53   PAF53 CAST

α-PAF53
(53 kD)   →Paf53

α-NOP1
(34kD)   →NOP1

F

FOA   −

Rpa49
−
Ppgk-PAF53
Ptef1-Paf53

rpa49Δ

G

+Caffeine   −

Rpa34
−
PAF53
CAST
PAF53 CAST

rpa34Δ

Figure 1. **PAF53/CAST heterodimer is functionally conserved from human to budding yeast.** (A) Pol I–specific subunits in *S. cerevisiae, S. pombe, Mus musculus*, and *Homo sapiens*. (B) Nucleolar localization of CAST depends on PAF53. CAST fused with YFP (YFP-CAST) is expressed in a WT yeast producing Nop1 fused to mCherry (mCherry-Nop1) with (PAF53) or without (−) PAF53 coexpression (see Materials and methods). (right) The overlay of both fluorescent signals (merge) is shown. (C) Immunoprecipitation of budding yeast Pol I demonstrates that association of CAST to Pol I requires human PAF53. HA-tagged CAST (HA-CAST) is detected in the supernatant (SUP) with or without coexpression of PAF53. Using IgG Sepharose to immunopurify TAP-tagged budding yeast Pol I (IP), CAST copurifies with Pol I only when coexpressed with PAF53 (+). Western blot using Pap and 12CA5 revealed tagged budding yeast Pol I (Rpa190-TAP) and CAST (HA-CAST) in supernatant (SUP) and immunoprecipitated fraction (IP), respectively. (D) Nucleolar localization of PAF53 depends on CAST. PAF53 fused with YFP (YFP-PAF53) is expressed in a WT budding yeast producing Nop1 fused to mCherry (mCherry-Nop1) with (CAST) or without CAST (−). CAST expression is required for both a detectable YFP signal and a nucleolar localization of PAF53. (E) PAF53 expressed

the rDNA is made of a 6.9-kb-long gene repeated ~150 times, of which about half is transcribed. Transcription of the rDNA is one to two orders of magnitude greater than the transcription of the rest of the genome. In exponentially growing cells, 0.01–10 Pol II enzymes are found per open reading frame (Bon et al., 2006), whereas >120 Pol I molecules can be detected (by Miller spread; Miller et al., 1969) at the transcribed region of each active rDNA repeat (Osheim et al., 2009).

Pol I activity is associated with the largest nuclear body, the nucleolus, where all earlier steps of ribosome biogenesis take place. Assembly of the nucleolus is proposed to be a self-organized process, initiated by production of rRNA (Trumtel et al., 2000; Misteli, 2001; Hernandez-Verdun et al., 2002). In budding yeast, Pol I is essential, but very elegant genetic analyses have been used to show that Pol II–dependent 35S rRNA expression, albeit very inefficiently, can rescue Pol I minus mutants (Nogi et al., 1991). Importantly, in mutant cells where Pol I is inactivated and Pol II is artificially producing rRNA, nucleolar structures are still detectable, but with massive alterations (Oakes et al., 1998; Trumtel et al., 2000). Therefore, rRNA synthesis achieved from its dedicated transcriptional apparatus is important for formation of the nucleolar structure.

In this study, we focus on the role of two Pol I–specific subunits, Rpa49 and Rpa34, in Pol I transcription and nucleolar morphology. Pol I lacking Rpa34/Rpa49 has been shown to be active in transcription but impaired in elongation (Huet et al., 1975). In vivo, *rpa49* and *rpa34* deletion mutants are viable, but are defective in 35S rRNA production (Liljelund et al., 1992; Gadal et al., 1997). Structural insight and biochemical assays have suggested that Rpa34/Rpa49 form a heterodimer behaving like built-in elongation factors (Kuhn et al., 2007). Another clue to Rpa49 function came from the observation that in *rpa49* deletion mutants, Rrn3 (TIF-IA in mouse), an essential Pol I transcription factor, is recruited to the promoter less efficiently and fails to dissociate from elongating polymerase (Beckouet et al., 2008). In this study, we demonstrate that the Rpa34/Rpa49 heterodimer is functionally conserved in evolution and required for nucleolar assembly. Using Miller spreads to analyze Pol I distribution in the absence of Rpa49 on single transcribed genes, we show that there is a decreased clustering of elongating Pol I complexes. 3D modeling of two neighboring Pol I complexes unveil how such association can regulate rRNA gene transcription cycle.

Results

The human hPAF53/CAST heterodimer is functionally conserved from human to budding yeast

We investigated the functional conservation of specific Pol I subunits from budding yeast to human (Fig. 1 A). In budding yeast, Rpa49 and Rpa34 are not essential for viability, and their amino acid sequences are poorly conserved through evolution. Orthologues of Rpa49 and Rpa34, PAF53 and PAF49 in mouse (Hanada et al., 1996; Yamamoto et al., 2004) and hPAF53 and CAST in human (also called ASE-1 or hPAF49; Panov et al., 2006), respectively, have a conserved domain organization with *S. cerevisiae* subunits but low sequence similarity. In budding yeast and mouse, Rpa49/Rpa34 orthologues are easily dissociated from the enzyme by high salt treatment (Huet et al., 1975; Hanada et al., 1996), and as a result, these two polypeptides have been classified either as Pol I–associated factors in mouse or as Pol I subunits in *S. cerevisiae* and human. A previous complementation attempt has established that *Schizosaccharomyces pombe* Pol I subunit Rpa51, hereafter called Sp-Rpa49, but not mouse PAF53, can complement *rpa49Δ* cold sensitivity (Nakagawa et al., 2003). Because Rpa49 and Rpa34 function as a heterodimer (Kuhn et al., 2007; Beckouet et al., 2008), we tested the coexpression of human CAST and hPAF53 in a complementation assay. We first investigated the localization of human CAST when expressed in wild-type (WT) budding yeast, with or without hPAF53 expression. CAST is nuclear when expressed alone but predominantly localized in the nucleolus when coexpressed with hPAF53 (Fig. 1 B). Starting from a yeast strain bearing a TAP-tagged Rpa190 (Rigaut et al., 1999), Pol I largest subunit, we purified Pol I to test the association of CAST with budding yeast Pol I. CAST is coimmunoprecipitated with budding yeast Pol I only when coexpressed with hPAF53 (Fig. 1 C). These results suggest that hPAF53/CAST heterodimer is replacing the Rpa49/Rpa34 heterodimer in budding yeast Pol I. We then investigated hPAF53 localization with or without CAST coexpression. No YFP-hPAF53 fusion protein was detected when it was expressed alone, but it was present in the nucleolus when coexpressed with CAST (Fig. 1 D). To test the idea that CAST stabilizes hPAF53 when coexpressed in budding yeast, we quantified hPAF53 by immunodetection in whole cell extracts with or without CAST (Fig. 1 E). hPAF53 is barely detectable in budding yeast extracts, even if expressed from the strong PGK1 promoter, but it accumulates

in budding yeast is stabilized by CAST coexpression. PAF53 is detected in a whole cell extract from WT budding yeast expressing PAF53 (PAF53) alone or coexpressed with CAST (PAF53 CAST) using PAF53 antibody (α-PAF53). Nop1 (α-Nop1) is used as loading control. Total extract from HeLa loaded in lane 1 is used as control for PAF53 detection. White lines indicate that intervening lanes have been spliced out. (F) Overexpressed PAF53 complements *rpa49Δ* cold-sensitive growth defect. 10-fold serial dilutions of *RPA49*-deleted strain expressing budding yeast RPA49 (Rpa49), empty vector (−), PAF53 expressed from a strong promoter (P_PGK-PAF53), or an even stronger budding yeast promoter P_TEF1 (P_TEF1-PAF53) were spotted on 5-FOA–containing plates to check for complementation of the mutant cold sensitivity at 25°C (see Materials and methods for plasmid-shuffling assay). Plates without FOA (−) are used as control to confirm that the same number of cells were spotted. The strength of the complementation is evaluated by comparing plates with (FOA) or without FOA (−). (G) Expression of the PAF53/CAST heterodimer complements the *RPA34* deletion phenotype. 10-fold serial dilutions of *rpa34* deletion strains containing budding yeast RPA34 (Rpa34), empty vector (−), PAF53 driven from a moderate promoter (PAF53), CAST expressed from the budding yeast promoter P_TEF1 (CAST) or coexpressing PAF53 and CAST (PAF53 CAST) were spotted on 1 g/liter caffeine-containing plates to check for suppression of the *rpa34Δ* mutant hypersensitivity. Strength of the suppression of drug sensitivity was evaluated by comparing plates with (+) or without (−) caffeine spotted with equivalent amount of cells.
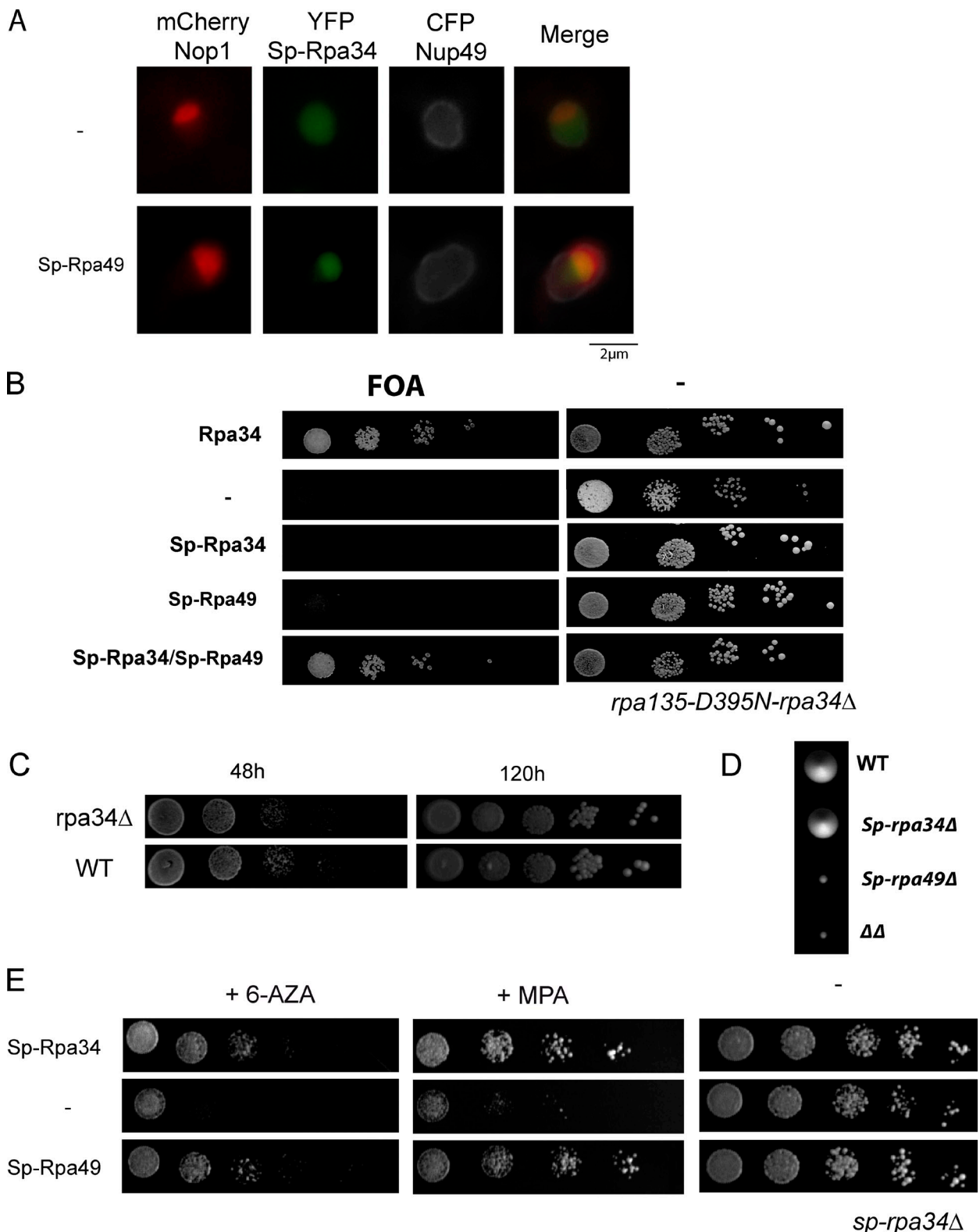
Figure 2. **Rpa49/Rpa34 heterodimer is conserved in fission yeast.** (A) In *S. cerevisiae*, nucleolar localization of Sp-Rpa34 depends on Sp-Rpa49. Sp-Rpa34 fused with YFP (YFP-Sp-Rpa34) is expressed in a WT budding yeast with (Sp-Rpa49) or without (−) Sp-Rpa49 coexpression. In all cases, cells produce Nop1 fused to mCherry (mCherry-Nop1) and Nup49 fused with CFP (CFP-Nup49) to label the nucleolus and the nuclear pore complexes, respectively. (right) Overlay of the three fluorescent signals (merge) is shown. (B) Sp-Rpa34/Sp-Rpa49 heterodimer complements budding yeast Rpa34 essential function in a Pol I mutant background (*rpa135-D395N*). 10-fold serial dilutions of *rpa34Δ rpa135-D395N* double-deletion strains containing *S. cerevisiae* *RPA34* (Rpa34), empty vector (−), Sp-Rpa34 (Sp-Rpa34), Sp-Rpa49 (Sp-Rpa49), or coexpressing Sp-Rpa34 and Sp-Rpa49 (Sp-Rpa34/Sp-Rpa49) were spotted on plates with (FOA) or without FOA (−), and complementation was evaluated by comparing plates with (FOA) or without FOA (−). (C) Sp-Rpa34 deletion barely affects growth in *S. pombe*. 10-fold serial dilutions of *S. pombe* WT and Sp-*rpa34* deletion strains in rich medium at 30°C after 48 (left) and 120 h (right). (D) *Sp-rpa34 Sp-rpa49* double deletion is viable in *S. pombe*. To generate the double-mutant strain, we crossed two haploid strains bearing

when coexpressed with CAST. Interestingly, CAST depletion in mouse and human cells leads to concomitant disappearance of PAF53, whereas the level of other Pol I subunits is unaffected (unpublished data). Therefore, our results suggest that coexpression of CAST and hPAF53 is required for hPAF53 stabilization.

We next tested the ability of the human subunits to complement the *rpa49Δ* and/or *rpa34Δ* phenotypes by plasmid-shuffling assays (see Materials and methods). hPAF53 on its own is unstable; therefore, we expressed hPAF53 under the control of the strong *PGK1* or the very strong *TEF1* promoter. *rpa49Δ* cold sensitivity was corrected by hPAF53 only when the pTEF1 promoter was used (Fig. 1 F). *rpa34Δ* has little growth defect, but it is hypersensitive to caffeine (1,3,7-trimethylxanthine; Beckouet et al., 2008). We assayed the ability of CAST, hPAF53, or both to suppress caffeine sensitivity. CAST and hPAF53 complemented the *rpa34Δ* mutant phenotype only when coexpressed (Fig. 1 G). Therefore, our results suggest that the CAST/hPAF53 heterodimer can substitute for the endogenous budding yeast Rpa49/Rpa34 within Pol I and can perform the function of the *S. cerevisiae* heterodimer in vivo.

The Rpa49/Rpa34 heterodimer is also conserved in fission yeast

Fission yeast Sp-Rpa49 can substitute for budding yeast Rpa49 (Nakagawa et al., 2003). A recent database search revealed that the *S. pombe* SPBC11G11.05 open reading frame (hereafter named Sp-Rpa34) has weak but significant sequence homology with Rpa34 (Beckouet et al., 2008). We cloned and expressed Sp-Rpa34 in budding yeast and observed its nucleolar localization only when coexpressed with Sp-Rpa49 (Fig. 2 A). Because of a slight toxicity of Sp-Rpa34 for *S. cerevisiae*, its effect on caffeine sensitivity of *rpa34Δ* was unclear. We next tested complementation by Sp-Rpa34/Sp-Rpa49 of the *rpa34Δ* mutant in an *rpa135-D395N* double-mutant background in which Rpa34 is essential for growth (Beckouet et al., 2008). When expressed alone, Sp-Rpa34 was unable to complement the Rpa34 essential function, but the coexpressed Sp-Rpa34/Sp-Rpa49 heterodimer restores growth (Fig. 2 B). Our results suggest that Sp-Rpa34 is the fission yeast counterpart of budding yeast Rpa34. We next deleted Sp-Rpa34 in *S. pombe*. The *Sp-rpa34Δ* mutant fission yeast was viable with only a slight growth defect (Fig. 2 C), similar to the *rpa34Δ* mutant in *S. cerevisiae*. Our previous data demonstrated that double-deletion mutants *rpa34Δ* and *rpa49Δ* are phenotypically equivalent to the *rpa49* single-deletion mutant and that Rpa49 overexpression can suppress the defects associated with *rpa34Δ* (Beckouet et al., 2008). The *Sp-rpa49Δ* single-deletion mutant and the double mutant *Sp-rpa49Δ Sp-rpa34Δ* grow similarly (Fig. 2 D). *Sp-rpa34Δ* has a strong sensitivity to mycophenolate and 6-azauracil compared with
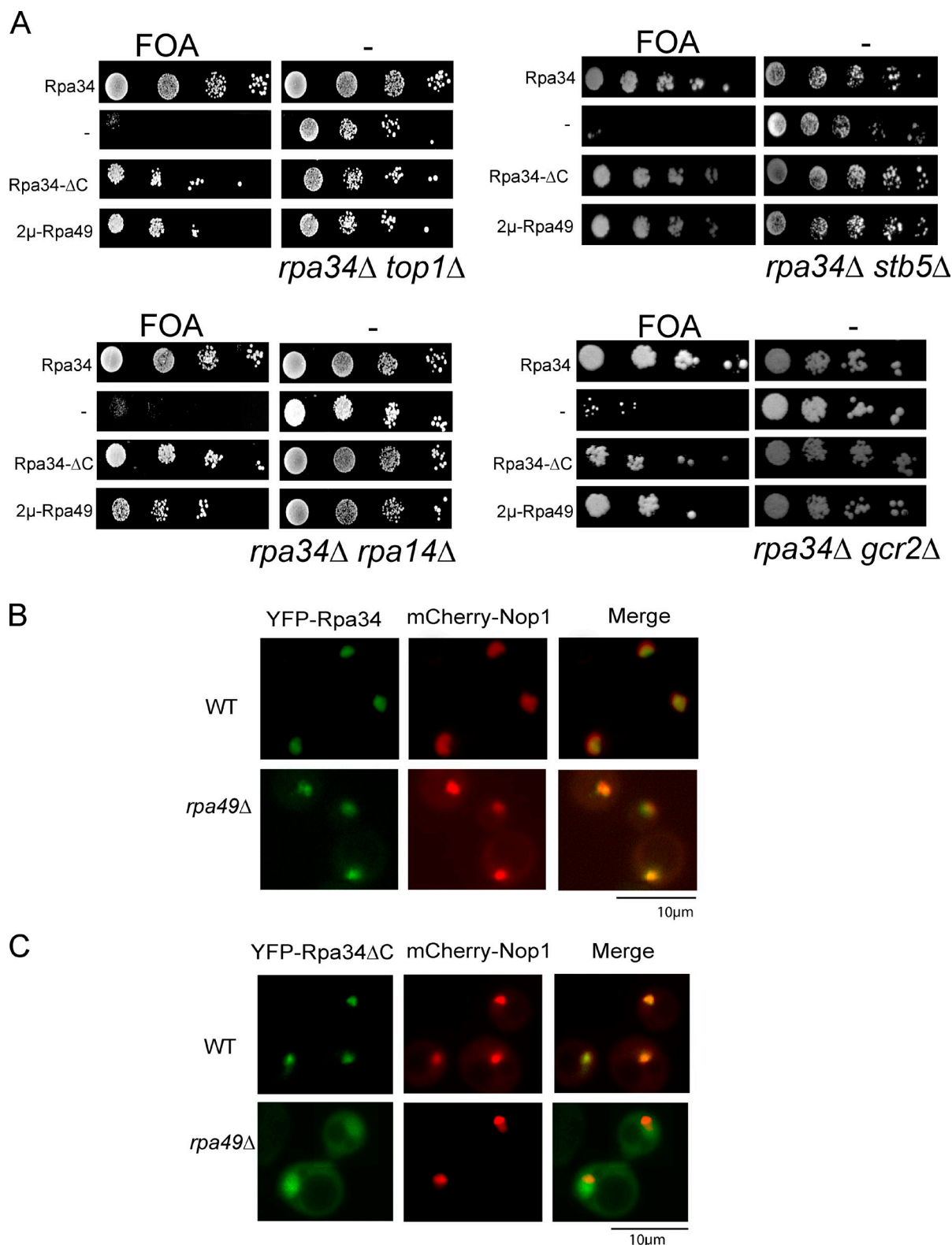
WT fission yeast. Both drugs deplete the pool of NTP in vivo and have a strong effect on strains with defects in RNA polymerase elongation. Sensitivity to both drugs is suppressed by overexpression of Sp-Rpa49 (Fig. 2 E). Therefore, our results strongly suggest that in *S. pombe*, both Pol I–specific subunits are conserved and functionally exchangeable with the budding yeast Rpa49/Rpa34 heterodimer.

The C-terminal domains of budding yeast Rpa34 contain a nucleolar localization signal

We showed that Rpa49 overexpression could suppress all known phenotypes of *rpa34Δ*, suggesting that Rpa34 function is restricted to stabilization of Rpa49 (Beckouet et al., 2008), but in higher eukaryotes, the orthologue of Rpa34 has several specific functions of its own (Yamazaki et al., 1999; Yamamoto et al., 2004; Panov et al., 2006). Our sequence analysis reveals that these polypeptides share a lysine-rich C-terminal domain. This domain is not required for interaction with Rpa49 (Beckouet et al., 2008), and we hypothesized that this feature could be responsible for a function unrelated to Rpa49. To verify this hypothesis, we decided to perform a search for all possible genetic backgrounds in which *rpa34Δ* is lethal. We performed a global genetic interaction mapping (GIM; Decourty et al., 2008) using *rpa34Δ* as bait. We confirmed two previously identified synthetic lethal interactions, *top1Δ* and *rpa14Δ* (Gadal et al., 1997), and identified two novel genetic backgrounds, *gcr2Δ* and *stb5Δ*, in which *rpa34* became essential (Fig. 3 A). However, Rpa49 overexpression could suppress the *rpa34Δ* phenotype in all tested backgrounds. Moreover, the truncated version of Rpa34 lacking the C-terminal domain was functional, revealing no growth phenotype associated with the absence of this particular domain.

We next tested whether the nucleolar localization of Rpa34 also depends on Rpa49 in budding yeast. In contrast to CAST and Sp-Rpa34, Rpa34 remains in the nucleolus even in the absence of Rpa49 (Fig. 3 B). We next tried to identify which domain of budding yeast Rpa34 could behave as a nucleolar localization signal functioning independently from Rpa49. The nucleolar localization of Rpa34 in Rpa49Δ background is lost upon truncation of the C-terminal domain (Fig. 3 C). The nucleolar targeting of Rpa34 C domain in *S. cerevisiae* appears to be species specific. Despite the apparent similarity between the C-terminal domains of Rpa34, CAST, and Sp-Rpa34, the nucleolar targeting of CAST and Sp-Rpa34 are strictly dependent on the coexpression of their respective binding partner, PAF53 or Sp-Rpa49. In contrast, Rpa34 in *S. cerevisiae* has two nucleolar targeting mechanisms. One depends on Rpa49 association, the other on the Rpa34 C-terminal domain.

the single *Sp-rpa34* or *Sp-rpa49* deletion. After meiosis, we analyzed the growth of single- and double-mutant offspring. Viability of the double mutant was confirmed in 20 tetrads. A representative tetratype tetrade is shown, with WT, single *Sp-rpa34*, or *Sp-rpa49* deletion and double *Sp-rpa34Δ Sp-rpa49Δ* (ΔΔ) genotype. (E) The sensitivity of the *Sp-rpa34* deletion strain to mycophenolic acid and 6-azauracil is suppressed by Sp-Rpa49 overexpression. 10-fold serial dilutions of *Sp-rpa34Δ S. pombe* expressing Sp-RPA34 (Sp-Rpa34), an empty vector (Sp-rpa34Δ), or overexpressing Sp-RPA49 (Sp-rpa34Δ + Sp-Rpa49) were spotted on rich media (left; −), 75 μg/ml 6-azauracil (middle; +6-AZA), or 40 μg/ml mycophenolic acid (right; +MPA) and grown for 4 d at 25°C.

A

FOA - FOA -

Rpa34
-
Rpa34-ΔC
2μ-Rpa49

rpa34Δ top1Δ *rpa34Δ stb5Δ*

FOA - FOA -

Rpa34
-
Rpa34-ΔC
2μ-Rpa49

rpa34Δ rpa14Δ *rpa34Δ gcr2Δ*

B

YFP-Rpa34 mCherry-Nop1 Merge

WT

rpa49Δ

10μm

C

YFP-Rpa34ΔC mCherry-Nop1 Merge

WT

rpa49Δ

10μm

Figure 3. **The C-terminal domain of Rpa34 is a nucleolar localization signal.** (A) Rpa34 C-terminal domain is fully dispensable in vivo. 10-fold serial dilutions of four double-mutant budding yeast strains, *rpa34Δ top1Δ* (top left), *rpa34Δ stb5Δ* (top right), *rpa34Δ rpa14Δ* (bottom left), or *rpa34Δ gcr2Δ* (bottom right), are shown. Double mutants containing RPA34 (Rpa34), empty vector (−), Rpa34-ΔC driven from a P_pgk1 promoter (Rpa34-ΔC), or overexpressing Rpa49 (2μ-RPA49) were spotted on 5-FOA–containing plates to check for complementation of the lethality of the double mutant. Plates were incubated for 3 d at 30°C. Strength of the complementation was evaluated by comparing plates with (FOA) or without FOA (−). (B) Nucleolar localization of Rpa34 is independent of Rpa49. Rpa34 fused with YFP (YFP-Rpa34) is expressed in a WT budding yeast or in a mutant lacking Rpa49 (*rpa49Δ*). Both strains produce Nop1 fused to mCherry (mCherry-Nop1). (right) Overlay of both fluorescent signals (merge) is shown. (C) Nucleolar localization of Rpa34-ΔC is dependent on Rpa49. Rpa34ΔC fused with YFP (YFP-Rpa34ΔC) is expressed in WT or in a mutant lacking Rpa49 (*rpa49Δ*). Both strains produce Nop1 fused to mCherry (mCherry-Nop1). (right) Overlay of both fluorescent signals (merge) is shown.

Rpa34 and Rpa49 influence nucleolar morphology

We have shown that the Pol I–specific Rpa49/Rpa34 heterodimer is functionally conserved from yeast to humans. We hypothesized that Pol I–specific subunits might be responsible for the two most prominent features of Pol I transcription: nucleolar assembly and high RNA polymerase loading rate per gene. We first focused on nucleolar alterations caused by the absence of Pol I–specific subunits. We labeled the nuclear periphery using GFP-Nup49, a nuclear pore protein, and the nucleolus using mCherry-Nop1, an abundant nucleolar protein, in WT, *rpa34Δ*, and *rpa49Δ* cells (Fig. 4 A). Nucleolar alterations in *rpa34Δ* and *rpa49Δ* cells were determined by thresholding the fluorescent nucleolar signal detected using confocal microscopy in a large number of cells (Berger et al., 2008). Because the cumulative distribution function accurately describes volume distribution in large samples, we used this representation to evaluate the nucleolar size for each mutant (Fig. 4 B). The nucleolar size increases considerably in *rpa49Δ* cells, suggesting that the integrity of nucleolar structure is compromised (Fig. 4 A). We next performed an ultrastructural study of the nucleus in *rpa49Δ* and *rpa34Δ* mutants. For optimal preservation of the nuclear structure, chemical fixation was avoided, and the cells were cryoimmobilized before low temperature substitution. The nucleolar ultrastructure is altered in both mutants (Fig. 4, C and D). In *rpa34Δ* cells, the nucleolus is decondensed with areas of low electron density. In *rpa49Δ* cells, the nucleolar morphology is dramatically altered: its characteristic crescent shape disappeared, and the dense material redistributed in the full volume of the nucleus.

Cryofixation also allows the direct observation of individualized cytoplasmic ribosomes. The number of ribosomes in *rpa34Δ* cells is similar with WT, but it is significantly reduced in *rpa49Δ* cells (Fig. 4 E). To investigate a defect in translation, we performed a polysome profile in WT and the *rpa49Δ* mutant. Interestingly, we detected polysomes in both backgrounds, but with the appearance of half-mers in *rpa49Δ* cells, reminiscent of a 60S biogenesis defect (Fig. 4 F). Such a defect was previously observed in a Pol I mutant strain defective for rRNA elongation (Schneider et al., 2007). Therefore, the morphological analysis demonstrates that Rpa49 is required for normal nucleolar morphology and efficient ribosome biogenesis. The *rpa49Δ* strain contains fewer 60S subunits relative to 40S, which is reminiscent of a Pol I elongation defect.

Reduction in the number of rDNA repeats can partially compensate for the alterations in nucleolar morphology caused by *RPA49* deletion
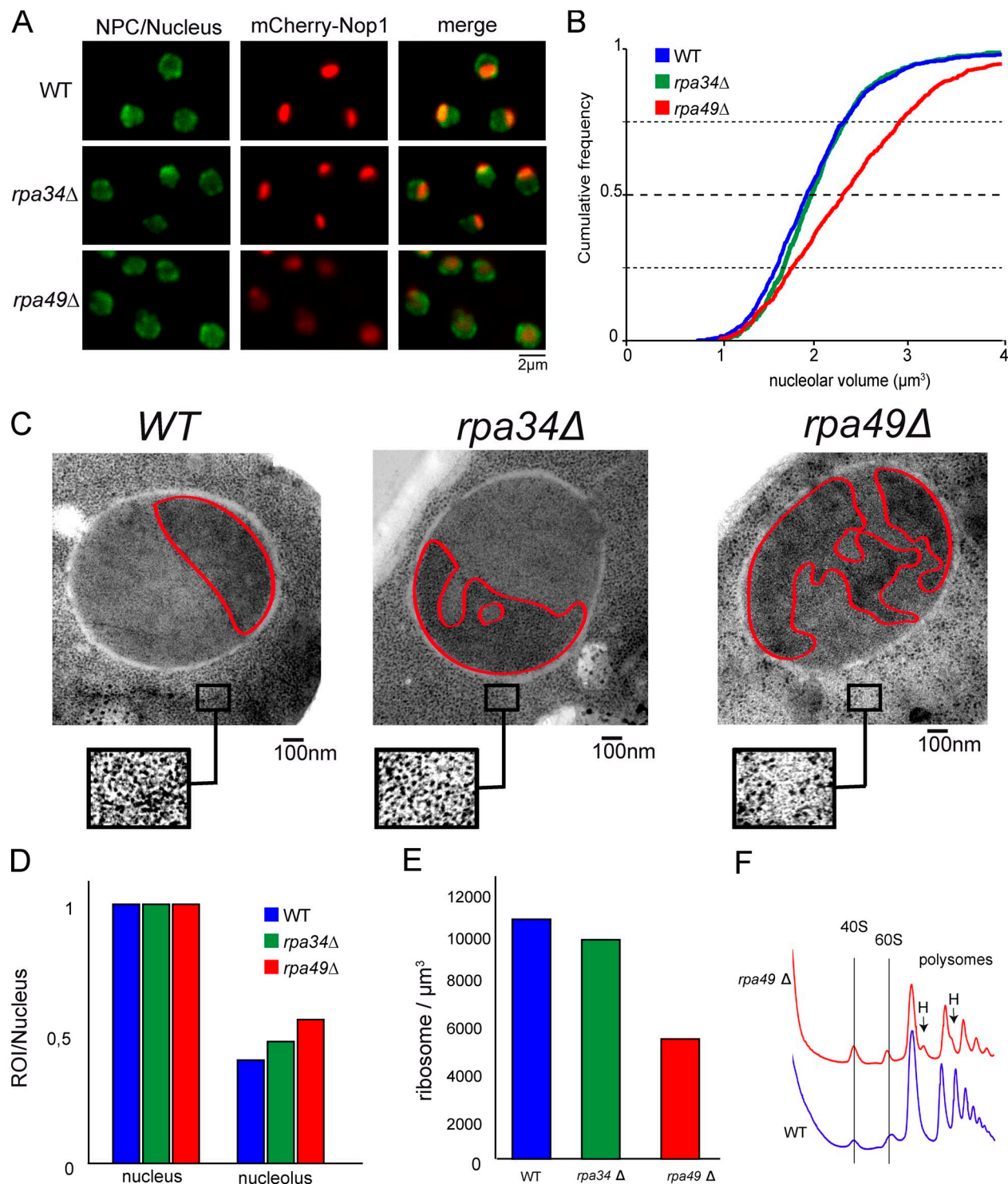
In the *rpa49Δ* mutant, rRNA production still sustains growth, but the nucleolus appears fully decondensed. To spatially constrain rRNA production, we decided to use mutant cells with a decreased number of rDNA repeats (Cioci et al., 2003). rDNA copy number can be stabilized at 25 copies by Fob1 deletion without significant growth defect (Cioci et al., 2003). To support normal rRNA production from such a low number of rDNA genes, the number of Pol I complexes per gene is significantly

increased (French et al., 2003). We first demonstrated that double-mutant *rpa49Δ fob1Δ* strains are viable at 30°C, having either 190 or 25 rDNA copies (Fig. 5 B). To confirm this surprising result, we establish that rDNA copy number in both strains is unaffected by *rpa49* deletion (Fig. 5 A). Growth of the *rpa49Δ* strain is severely impaired at 25°C (Liljelund et al., 1992). Comparing growth of the *rpa49Δ fob1Δ* strains containing 25 versus 190 rDNA copies, we noted that the cold sensitivity is alleviated upon reduction in the number of rDNA repeats (Fig. 5 B).

Quantitative fluorescence analysis revealed that in presence of Rpa49, the reduction from 190 to 25 rDNA copies resulted in a nucleolus of normal size (Fig. 5 C). Electron microscopy observations showed that the nucleolus in the 25 rDNA copies background is characterized by an identifiable crescent-shaped area of fibrillo-granular material adjacent to the nuclear envelope (Fig. 5 D). Interestingly, in the Rpa49 deletion strain with 25 rDNA copies, but not with 190 copies, a crescent-shaped nucleolus is detectable in most cells (60%), as evaluated by fluorescence microscopy (Fig. 5 C). Similarly, the nucleolar morphology is partially restored at the ultrastructural level because a dense structure occupying one third of the nuclear surface and in contact with the nuclear envelope can be detected (Fig. 5 D). These data suggest that a decrease in the rDNA copy number is enough to establish a partial nucleolar organization in the absence of Rpa49.

RNA Pol I distribution on single genes is dependent on Rpa49

Having shown that nucleolar assembly is dependent on Rpa49, we next evaluated whether a high RNA Pol I loading rate per gene requires Rpa49. Miller spreads are the only technique allowing counting of individual Pol I on a single gene (Miller et al., 1969). However, the ability to quantify and accurately localize polymerase on a single gene relies on obtaining high contrast chromatin spreads from mutant yeast cells. The chromatin spreading technique was set up in our laboratory using strain NOY886, which contains 42 actively transcribed rDNA copies (Fig. 6 A; French et al., 2003). Because of the very high loading rate in mutant backgrounds with reduced rDNA copy number, polymerases often appear as a continuous track, making accurate counting of single polymerases difficult. We took advantage of negatively stained Miller spreads obtained with low frequency (see Materials and methods) to demonstrate that continuous tracks are best analyzed by assuming the presence of a polymerase every 12 nm along such track (Fig. 6 C). We next analyzed Pol I density and distribution on the rRNA genes in 25 or 190 rDNA copy strains with or without Rpa49 using Miller spreads (Fig. 7 A). In the presence of Rpa49, we observed 62 ± 11 Pol I complexes per single rRNA gene in the 190 rDNA copy strain. However, in this strain, we were unable to identify rDNA in chromatin spreads in the absence of Rpa49, probably because of a very low Pol I occupancy of the rDNA. We next analyzed chromatin spreads in strains with 25 rDNA copies and identified single transcription units both in the presence and absence of Rpa49 (Fig. 7 A). We detected 122 ± 17 Pol I complexes per gene in the presence of Rpa49 and 36 ± 5 Pol I

Figure 4. **Rpa34 and Rpa49 are required for nucleolar integrity.** (A) Nucleolar structure of *rpa49Δ* and *rpa34Δ* cells assessed by fluorescent microscopy. Representative confocal sections of strains TMS1-1a (WT), BEN18-1a (*rpa34Δ*), and BEN19-1a (*rpa49Δ*) expressing TetR-GFP staining the nucleus, GFP-Nup49 staining the NPC (NPC/nucleus), and mCherry-Nop1 staining the nucleolus (mCherry-Nop1) are shown. (right) Overlay of both fluorescent signals (merge) is shown. (B) Cumulative distribution function of the nucleolar volume in Pol I mutants. The nucleolar volume was estimated by thresholding using the intensity of the mCherry fluorescent signal in WT, *rpa49Δ*, and *rpa34Δ* mutant cells (n_{WT} = 907; n_{rpa49} = 620; n_{rpa34} = 928). (C) Ultrastructural study of cryofixed, cryosubstituted WT, *rpa34Δ*, and *rpa49Δ* budding yeast cells. Representative sections of the nuclei are depicted, with manual segmentation of nucleolus bounded by red lines. The cytoplasmic ribosomal contents in the three budding yeast strains are depicted in a selected frame. (D) Quantification of ultrastructural morphological alterations in Pol I mutants. Nucleolar area normalized by nuclear surface is estimated by manual segmentation of electron microscopy sections (n = 20). (E) Quantification of the ribosomal cytoplasmic content in Pol I mutants. Ribosomal content of representative sections (n = 20) was manually counted and expressed as ribosomes per micrometer cubed. (F) Polysomal profiles (OD_{260} nm) after sucrose density gradient centrifugation derived from the *rpa49Δ* mutant and WT strain. The positions of 40S ribosomal subunits, 60S ribosomal subunits, polysomes, and half-mer polysomes (H) are indicated.
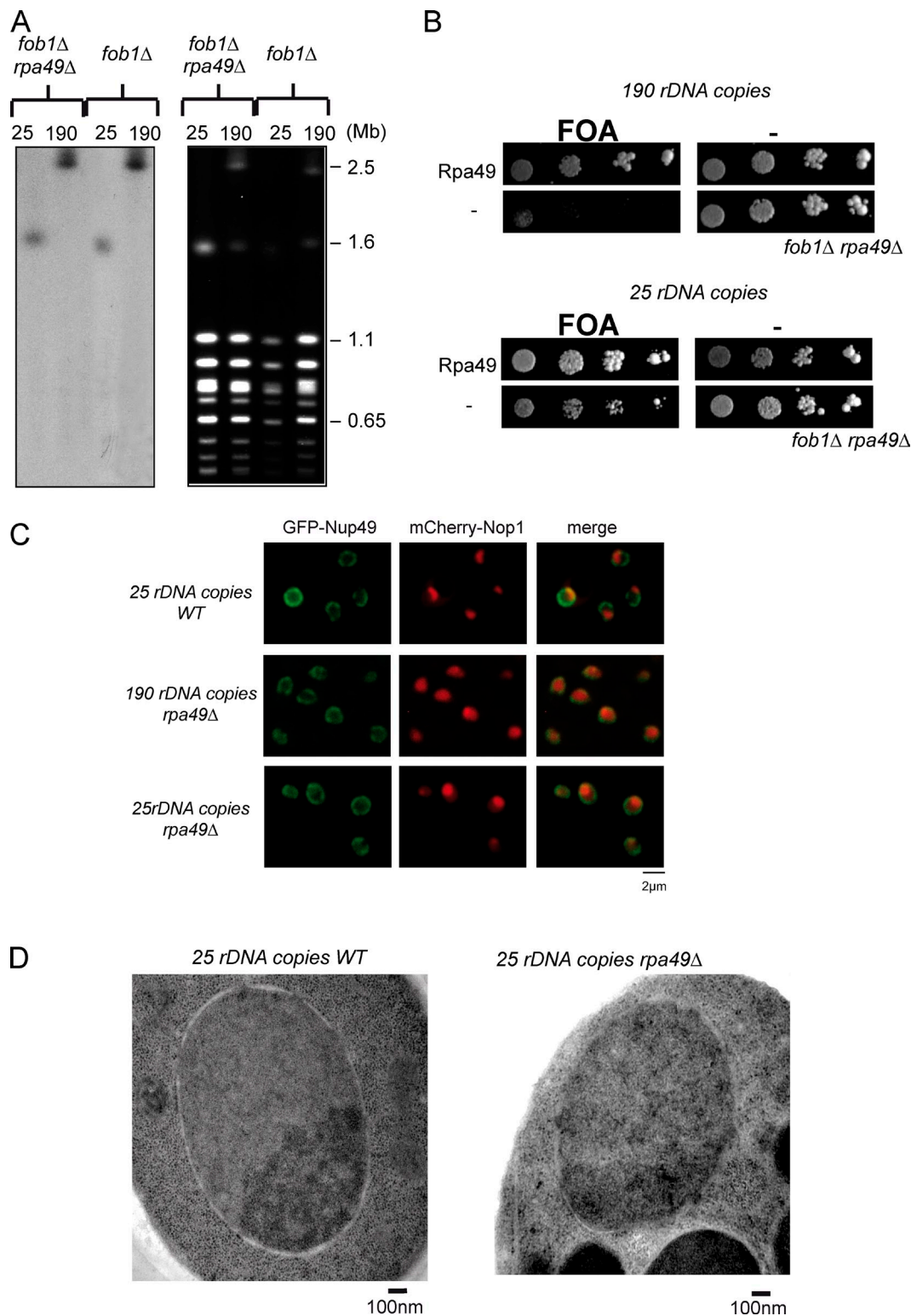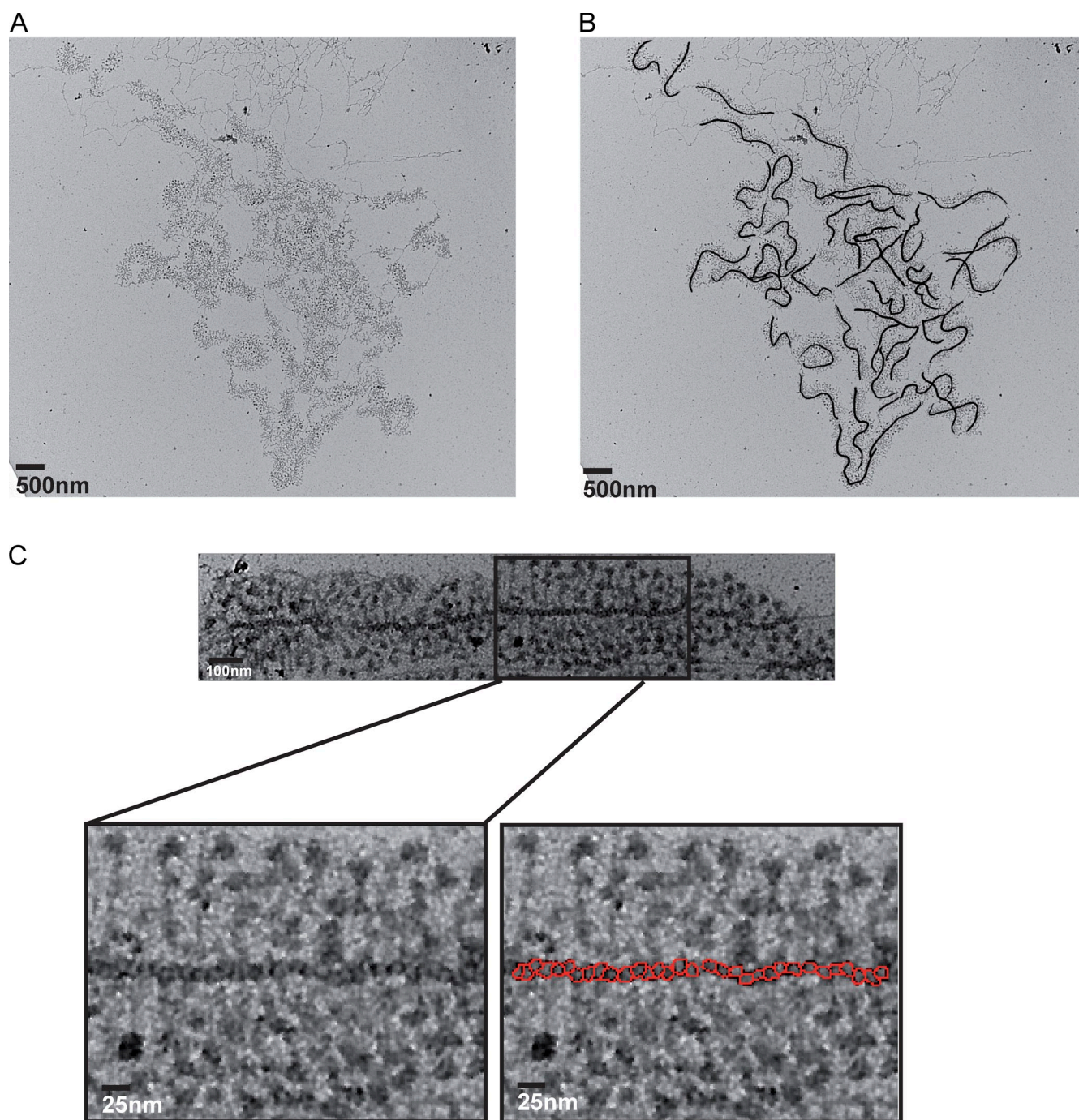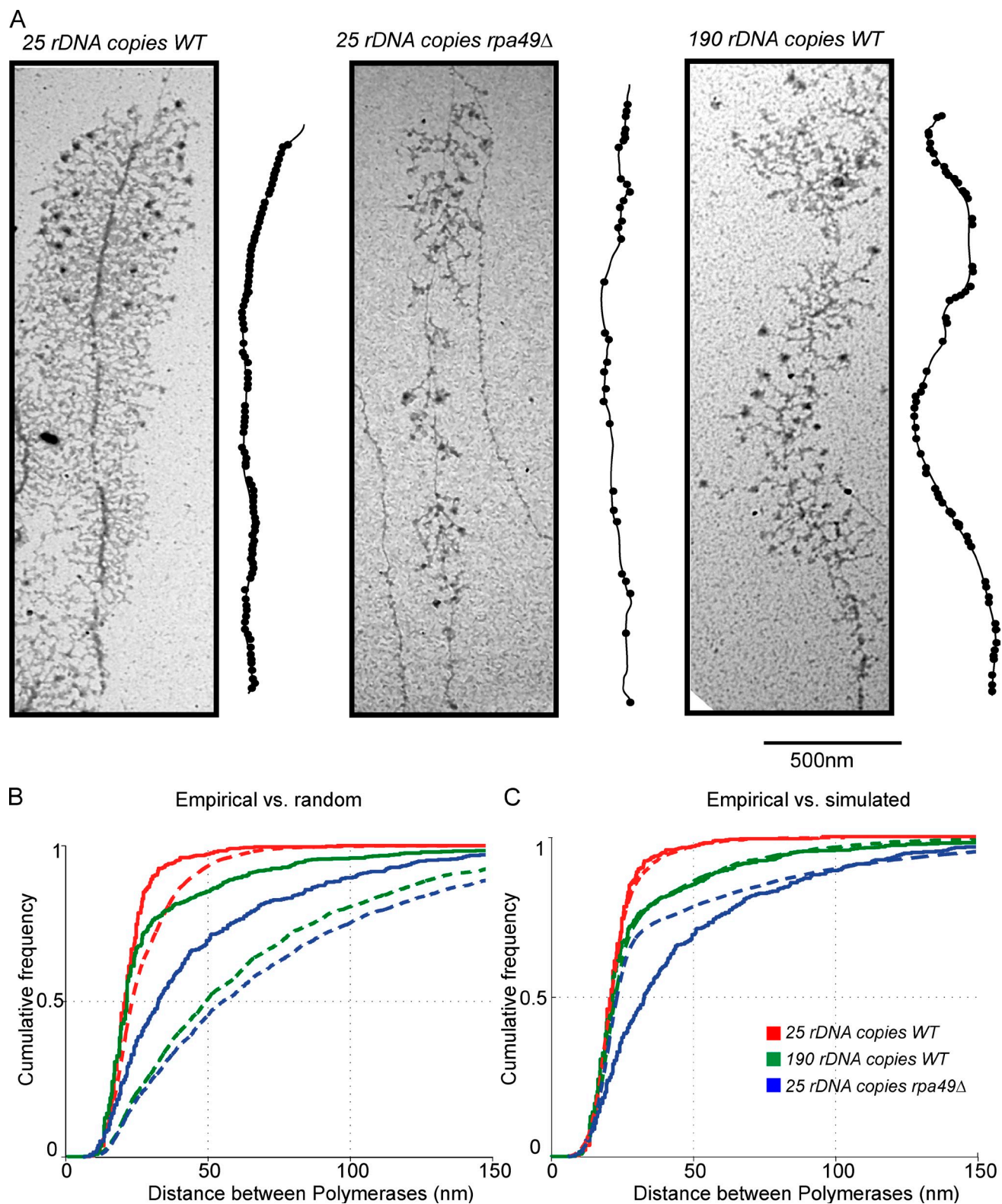
Figure 5.   **rpa49Δ phenotype in strains with 190 or 25 copies of rDNA.** (A) rDNA copy number is unaffected by *rpa49* deletion in a *fob1* deletion background. PFGE of chromosomes from *rpa49Δ fob1Δ* strains resulting from invalidation of the *rpa49Δ* gene in *fob1Δ* strains containing either 25 or 190 copies of rDNA or from original *fob1Δ* strains. Separated chromosomes were stained with ethidium bromide (right). Hybridization of rDNA probes was performed to estimate chromosome XII size (left). (B) Growth phenotype of the *fob1Δrpa49Δ* double-mutant strains bearing 190 or 25 copies of rDNA. 10-fold serial dilutions of strains BEN20-1a (25 rDNA copies *rpa49Δ fob1Δ*) and BEN21-1a (190 rDNA copies *rpa49Δ fob1Δ*) deleted for *rpa49* and containing 25 or 190 copies, respectively, of rDNA and an empty vector (−) or bearing *RPA49* (Rpa49) were spotted on plates with (FOA) or without FOA (−) and grown at 25°C for 7 d. (C) Nucleolar structure of Pol I mutants assessed by fluorescent microscopy. Representative confocal sections of strains NOY1071 (25 rDNA copies *fob1Δ*), NOY1064 (*190 rDNA copies rpa49Δ*), and BEN20-1a (25 rDNA copies *rpa49Δ*) containing GFP-Nup49 staining the NPC (GFP-Nup49) and mCherry-Nop1 staining the nucleolus (mCherry-Nop1). (right) Overlay of both fluorescent signals (merge) is shown. (D) Ultrastructural study of cryofixed, cryosubstituted strains with 25 rDNA copies with (WT) or without Rpa49 (*Rpa49Δ*).
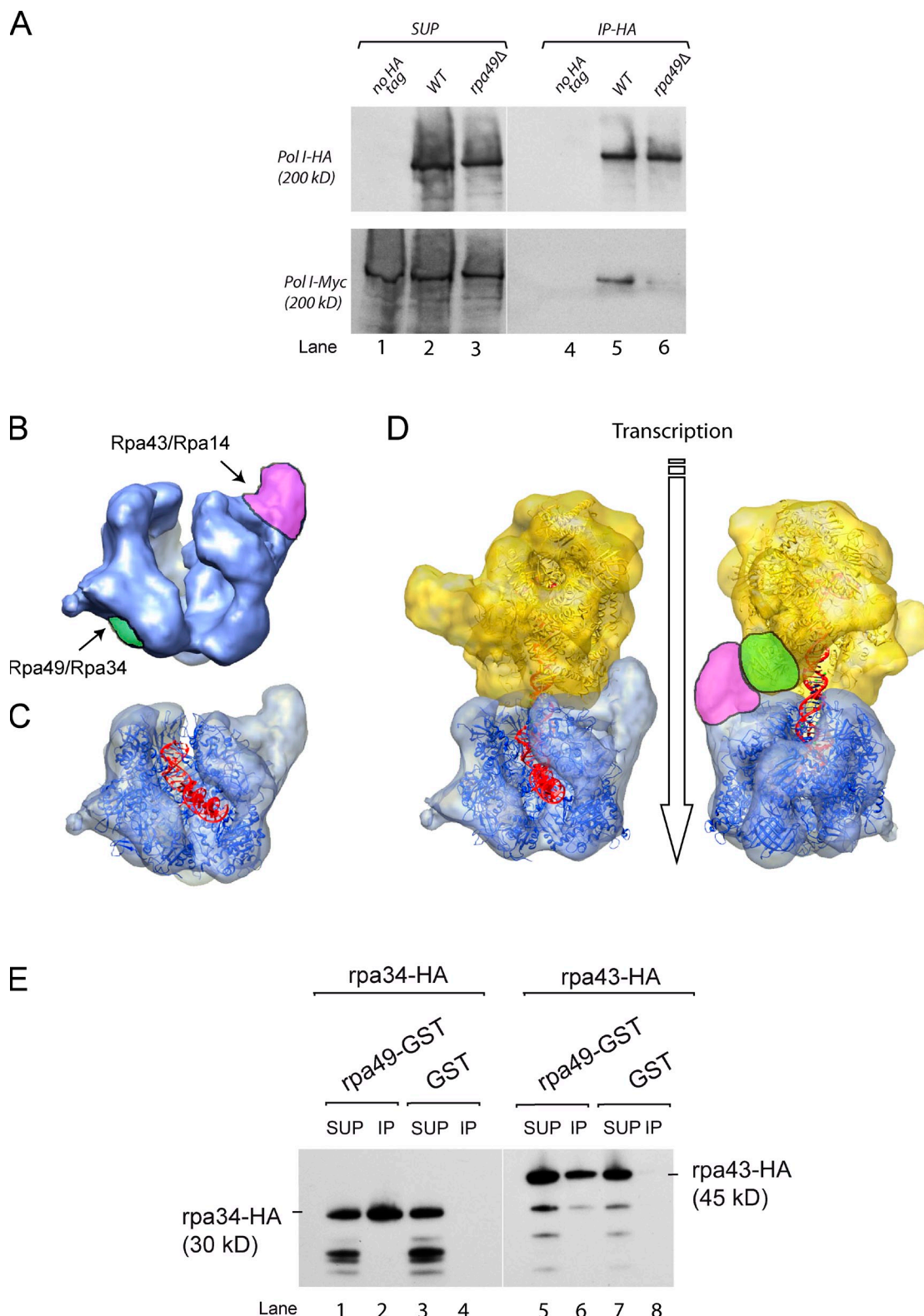
A

B

C

Figure 6. **Quantification of polymerases along transcribed rDNA genes.** (A) Visualization of active genes in rDNA. Using a mutant strain with a reduced number of rDNA copies (strain NOY886; 42 rDNA copies), we obtained high quality spreads from total nucleolar DNA. (B) Quantification of actively transcribed rDNA genes. The quantification of active genes in mutant strain (42 active gene in NOY886) is compatible with previous results (French et al., 2003). (C) Visualization of individual polymerases on negatively stained Miller spread. In mutant strains with 25 rDNA copies, Pol I density on each gene is very high. Using higher magnification (bottom left), we can still detect individual polymerases, which can be quantified (right; red circles). Note that a nascent rRNA can be visualized from each detected polymerase.

complexes per gene in its absence. We then measured the distance between adjacent polymerases to evaluate whether the Pol I molecules were randomly distributed on the rRNA genes (Fig. 7 B). The distances between polymerases depend intrinsically on the Pol I density on each rRNA gene, which varies between strains. Therefore, for each polymerase load, we first compared the empirical measurements of distance between polymerases with the corresponding random distribution predicted (Fig. 7 B). In all cases, the observed distance between polymerases was shorter than that predicted for the random distribution. These results suggest clustering of polymerases. We have introduced a new parameter in our simulations to take this effect into account. When 60% of polymerases are modeled as being in direct contact with each other and 40% are randomly

Figure 7. **Miller spread of 190 and 25 rDNA copy strains with or without Rpa49.** (A) Representative Miller spread from NOY1071 bearing 25 rDNA copies (25 rDNA copies [WT]), BEN20-1a bearing 25 rDNA copies and rpa49Δ (25 rDNA copies [rpa49Δ]), and NOY1064 bearing 190 rDNA copies (190 rDNA copies [WT]). (right) Interpretive tracing of the genes is shown. Polymerases that appear on the gene are shown on the tracing by black dots. (B and C) Cumulative distribution function of the distances between adjacent polymerases in strains NOY1071 (red; 25 rDNA copies [WT]), BEN20-1a (blue; 25 rDNA copies [rpa49Δ]), and NOY1064 (green; 190 rDNA copies [WT]) is shown. Solid lines, empirical measurement; dashed lines, random (B) or simulated (C).

Figure 8. **Two successive elongating Pol I complexes allow a contact between Rpa49 and Rpa43 subunit of adjacent molecules.** (A) Frequent association of adjacent Pol I depends on Rpa49. We generated diploid cells expressing two versions of Pol I containing an Rpa190 subunit fused to either the Myc or HA tag. These tagged proteins are efficiently detected in cell extract supernatants (SUP). After formaldehyde cross-linking and extensive DNase treatment, we immunoprecipitated Pol I using anti-HA antibodies (IP). We evaluated the amount of polymerase dimers/multimers by assessing the extent of Myc-tagged Rpa190 coprecipitation. We use a strain bearing only Myc-Tag Pol I as negative control (no HA tag; lanes 1 and 4). The presence of dimers/multimers is dependent on Rpa49, as shown by lack of Myc-tagged Rpa190 coimmunoprecipitation in *rpa49* deletion background (*rpa49Δ*; compare lanes 5 and 6) (B) 3D model of Pol I as determined by cryo–electron microscopy. The positions of the Pol I–specific Rpa43/Rpa14 and Rpa49/Rpa34 heterodimers are shown in purple and in green, respectively. (C) Fitting of the atomic structure of the highly homologous Pol II elongation complex (Protein Data Bank accession no. 2YU9) into the cryo–electron microscopy structure of RNA Pol I. The transcribed DNA is shown in red, and the 10-subunit core Pol II is shown in blue.

distributed, the simulated data are in good agreement with our experimental measurements in the case of the 190 and 25 rDNA copy strains in the presence of Rpa49 (Fig. 7 C). However, in the 25 rDNA copy/*rpa49Δ* strain, we measured larger distances between polymerases compared with the predictions of the model. Therefore, we propose that the interactions between successive Pol I complexes are strongly reduced in the absence of Rpa49, accounting for the reduction in the number of adjacent Pol I complexes. Therefore, Rpa49 is required to ensure high density of Pol I per rDNA gene. Furthermore, our data suggest that Rpa49 is involved in establishing contact between adjacent Pol I complexes.

Molecular modeling of contacts between adjacent polymerases on rDNA genes

Rpa49 seems to be required for interaction between adjacent transcribing polymerases. To confirm the requirement on Rpa49 for contact between adjacent polymerases, we coexpressed in a single diploid cell two of Pol I complex's largest subunits tagged with different epitopes, Myc and HA. By purifying HA-tagged Pol I from the chromatin-bound fraction, we could evaluate the amount of polymerase dimers or multimers by assessing the extent of copurification of Myc-tagged Pol I. In WT cells, after formaldehyde cross-linking and with extensive DNase treatment, we could detect frequent Pol I dimers (Fig. 8 A). In absence of Rpa49, the proportion of Pol I dimers or multimers is dramatically reduced (Fig. 8 A, compare lane 5 with lane 6).

Using Miller spreads and coimmunoprecipitations, we show that elongating Pol I enzymes are in frequent contact in an Rpa49-dependent manner. To characterize potential molecular interactions occurring between successive polymerases, we modeled the structure of a Pol I dimer in an elongation state on DNA (Fig. 8 D). We used a cryo–electron microscopy density map of Pol I obtained as described previously (De Carlo et al., 2003) onto which the Rpa43 and Rpa49/Rpa34 heterodimer are localized far away from each other in different parts of the Pol I complex (Fig. 8 B; Bischler et al., 2002; Kuhn et al., 2007). To model the DNA upstream and downstream of the Pol I transcription bubble, we used the atomic structure of the corresponding RNA Pol II elongation complex (Protein Data Bank accession no. 2YU9; Fig. 8 C; Wang et al., 2006). A second elongation complex was then positioned according to the following constraints: (a) enzymes were placed in contact, (b) the intervening DNA connecting the two polymerases was set as linear, and (c) this linker DNA was modeled as B-DNA to find the rotational register between the two elongating polymerases (Fig. 8 D). The minimal distance between two successive active sites was found to be of 34 bp, which is in good agreement with

ExoIII footprinting experiments on RNA Pol II elongation complexes (Samkurashvili and Luse, 1998). Interestingly, in this model, the Rpa49/Rpa34 subunits of one polymerase are brought in close proximity to the Rpa43/Rpa14 heterodimer of the following Pol I. Genetic evidence previously suggested that Rpa49 and Rpa43 are functionally linked (Beckouet et al., 2008). To test whether Rpa49 directly associates with Rpa43, we coexpressed GST-tagged Rpa49 and HA-tagged Rpa43 in *Escherichia coli*. Because Rpa49 and Rpa34 form heterodimers, we used GST-tagged Rpa49 and HA-tagged Rpa34 as positive controls. Upon purification on glutathione Sepharose beads, both Rpa34 and Rpa43 copurify with GST-Rpa49 (Fig. 8 E, lanes 2 and 6). In contrast, HA-tagged Rpa43 or HA-tagged Rpa34 are not copurified with GST alone (Fig. 8 E, lane 4 and 8). Therefore, genetic and biochemical assays suggest a direct interaction between Rpa43 and Rpa49.

Discussion

In this study, we addressed the function of two Pol I-specific subunits, Rpa49 and Rpa34. We showed that heterodimers formed by human or fission yeast orthologues are functional in budding yeast, demonstrating a functional conservation of these two Pol I–specific subunits in the course of evolution. We also showed that these subunits are playing an important role in the formation of the nucleolus and are required to produce a high density of elongating Pol I on rDNA genes.

RNA Pol I evolutionary conservation

All eukaryotic cells exploit three distinct RNA polymerases to transcribe their nuclear genome. Of these, Pol I is the most divergent enzyme, probably because of its highly specialized function: it transcribes only a single gene encoding large rRNAs. Our data demonstrate that despite considerable variation in sequence, two of the Pol I–specific subunits forming a heterodimer, Rpa49/Rpa34, have orthologues throughout the eukaryotic domain, suggesting that functions of this dimer are evolutionally conserved. Our results show that overexpression of Rpa49 can rescue the growth defects in genetic backgrounds in which *rpa34Δ* is lethal. The C-terminal domain of Rpa34 is responsible for nucleolar localization, and it functions independently from Rpa49. Nucleolar localization sequences are known to interact with various nucleolar factors (Lechertier et al., 2007), suggesting the possibility of a direct interaction between the C-terminal domain of Rpa34 and *S. cerevisiae* nucleolar proteins. Indeed, several potential partners of Rpa34 have been identified in an unbiased two-hybrid interaction screen between Rpa34 and the complete genome. In this screen, three nucleolar

(D) Positioning of a second Pol I elongation complex (yellow) following a leading Pol I elongation complex (blue) by imposing a straight B-form linker DNA and a contact between the Pol I molecules. The black arrow represents the direction of RNA Pol I translation during elongation. (left) The model is rotated 180° around the vertical axis as compared with the right panel. (E) HA-tagged Rpa43 and Rpa34 bind to GST-tagged Rpa49 when expressed in *E. coli*. Expression and purification of recombinant GST-Rpa49 or GST alone in the presence of HA-tagged Rpa34 or Rpa43 is described in Materials and methods. The supernatants of *E. coli* cell lysates (SUP) were incubated with glutathione Sepharose 4B beads. After washing, GST-Rpa49 and GST were eluted with sample buffer (IP), and the fractions were analyzed by Western blotting to detect coprecipitation of HA-tagged Rpa34 (lanes 1–4) or Rpa43 (lanes 5–8). In the supernatant fractions, we detect full-length HA-Rpa34 and HA-Rpa43 and minor degradation products. Note that Rpa34 and Rpa43 appear specifically enriched in samples containing affinity-purified GST-Rpa49 compared with GST alone (compare lane 2 with lane 4 for Rpa34; compare lane 6 with lane 8 for Rpa43). White lines indicate that intervening lanes have been spliced out.

proteins, Gno1, a cofactor of the RNA helicase Prp43, and two components of the C/D snoRNP complexes Nop56 and Nop58 were shown to interact with Rpa34 (Beckouet et al., 2008). Therefore, the C-terminal domain is involved in the recruitment of species-specific binding partners, which are responsible for nucleolar targeting.

Pol I transcription influences nucleolar morphology

The nucleolus is the largest nuclear domain, the integrity of which depends directly on rRNA production (Trumtel et al., 2000; Hernandez-Verdun et al., 2002). This structure is conserved in all eukaryotes, and most nuclear steps of ribosome biogenesis take place within the nucleolus. In the absence of Rpa34 and especially Rpa49, nucleolar assembly is severely compromised. Importantly, the altered nucleolar morphology in *rpa49*-null strains correlates with a significant reduction in the number of ribosomes per cell. When we artificially decreased the number of rDNA copies from 190 to 25, in the absence of Rpa49, we observed a partial nucleolar reassembly. Therefore, we propose that the initial event required for self-organization of the nucleolus is a spatially constrained rRNA synthesis, which initiates the chain of events leading to formation of nucleolar structures.

Function of the Rpa49/Rpa34 heterodimer in Pol I transcription

A previous study revealed a close relationship between Rrn3, the two heterodimers Rpa49/Rpa34, and Rpa43/Rpa14 (Beckouet et al., 2008). The release of the Pol I–specific initiation factor Rrn3 during elongation requires Rpa49, despite diametrically opposite locations within a single Pol I complex (Beckouet et al., 2008). While our work was in progress, an elegant structural study established that the Rpa49 and Rpa34 heterodimer binds DNA and stimulates polymerase-intrinsic RNA cleavage (Geiger et al., 2010). We now show that Rpa49 is required to allow contact between adjacent polymerases. 3D modeling of adjacent contiguous polymerases gives a hint as to how Rrn3 could be released. Rrn3 and its interacting partner Rpa43 are in direct contact with Rpa49/Rpa34 of the neighboring enzyme. Indeed, we know that mutations of Rpa43 behave as extragenic suppressors of the *rpa49Δ* phenotype, and Rpa49 and Rpa43 when coexpressed in *E. coli* are interacting, arguing for a physical contact between both subunits (Beckouet et al., 2008).

From our model, we propose that adjacent polymerases form a head to tail "camel caravan" in which Rpa49 from one Pol I molecule is in direct contact with Rpa43 from the neighboring molecule. These interactions determine the distance between successive Pol I complexes. In the absence of Rpa49, adjacent complexes are unable to interact, and this could lead to the lack of Rrn3 release (Beckouet et al., 2008) and to the increased distance between polymerases (this study). All of these data together strongly suggest that the two Pol I–specific subunits Rpa49 and Rpa34 are essential for nucleolar assembly and formation of "Pol I caravans," two unique Pol I features. We now need to understand how contacts between adjacent Pol I, promoted by Rpa49, could affect yeast nucleolar integrity, impacting on rDNA organization in the nuclear space.

Materials and methods

Yeast strains, plasmid construction, and plasmid-shuffling assays

Yeast strains used in this study are listed in Table S1, and oligonucleotides are listed in Table S2. Yeast strains were constructed by meiotic crossing and plasmid DNA transformation. *S. cerevisiae*–null alleles with KanMX4 insertions were obtained from EUROSCARF and were checked using ad hoc PCR amplifications. The *Sp-rpa34Δ* gene deletion in *S. pombe* strain BENSP1-1a was performed by homologous recombination using PCR-amplified fragments with oligos 746 and 747 with plasmid p29802 as template. *Sp-Rpa49Δ* (*rpa51Δ*) was obtained as previously described using plasmid pYN1003usds (Nakagawa et al., 2003). pDONR201 (Invitrogen), pREP41 (Basi et al., 1993), pRS413, pRS423, pRS425 (Sikorski and Hieter, 1989), pVV200, pVV208 (Van Mullem et al., 2003), p29802, pUN100-mCherry-NOP1 (mCherry-NOP1) and pASZ11-CFP-NUP49 (CFP-NUP49; Berger et al., 2008), pFL36-CII, pGID-CII (Berger et al., 2007), pOG5-RPA34 (Gadal et al., 1997), pENTR-PAF53, pENTR-CAST, pENTR-HA-CAST (Panov et al., 2006), pOG1-A34 (Beckouet et al., 2008), pENTR-RPA49 (Beckouet et al., 2008), pYN1003usds (Nakagawa et al., 2003), and pNOY373 (Wai et al., 2000) were previously described. pEB5 and pENT-Rpa34DC58 were provided by E. Bertrand and F. Beckouët, respectively.

pRS425-P_{PGK} was constructed by ligating the NdeI fragment from pVV200 in the SmaI site of pRS425. pCNOD08, a gateway vector that allows strong transcription from the *TEF1* promoter, was constructed in three steps. First, the 1,281-bp XhoI–NcoI fragment of pRS425-P_{PGK} containing promoter P_{PGK} and *attR1* lambda recombination site was inserted into XhoI and NcoI–digested vector pFSKB3X (GTP technology) to generate plasmid pCNOD02. Second, promoter P_{TEF1} was amplified by PCR using oligonucleotides 439 and 440 and yeast ODN1-1a genomic DNA as template. The XbaI–XhoI-digested PCR product was cloned into the same site of pCNOD02 to generate plasmid pCNOD05. The 1,281-bp NcoI–XhoI fragment of pCNOD05 was inserted into pRS425-pPGK digested with NcoI and XhoI generating pCNOD08. pRS423-P_{PGK} was constructed by subcloning the DraIII–SacI fragment from pRS425-P_{PGK} in the same site of pRS423. pCFP-Nup49-His was constructed by ligating the HindIII (filled in with Klenow) to SacI in the SmaI–SacI of pRS413. pREP41-gat was made a gateway destination vector by ligating the PCR-generated fragment using oligos 740 and 741 and pRS425-P_{PGK} as the template, cut VspI–XhoI inserted in NdeI–SalI of pREP41. The following plasmids were constructed using Gateway technology (Invitrogen): (a) pENTR-Rpa34, by a BP reaction with pDONR201 and PCR-generated fragment amplified using oligonucleotides 463 and 464 and genomic DNA from *S. cerevisiae* strain ODN1-1a as a template, and (b) pENTR-Sp-Rpa34 and pENTR-Sp-Rpa49, by a BP reaction with pDONR201 and PCR fragment generated using oligonucleotides 742–743 or 744–745, respectively, and genomic DNA from *S. pombe* strain TG11 as template. pRS425-P_{PGK}-CAST, pRS425-P_{TEF1}-CAST (Ptef1-CAST), pVV200-CAST, pEB5-CAST (YFP-CAST), pRS425-P_{PGK}-HA-CAST, pEB5-PAF53 (YFP-PAF53), pRS423-P_{PGK}-PAF53, pRS425-P_{PGK}-PAF53, pVV200-PAF53 (P_{PGK}-PAF53), pRS425-P_{TEF1}-PAF53 (P_{TEF1}-PAF53), pRS425-Sp-Rpa49, pVV200-Sp-Rpa49, pREP41-Sp-Rpa49, pEB5-Sp-Rpa34 (YFP-Sp-Rpa34), pRS425-P_{PGK}-Sp-Rpa34, pVV200-Sp-Rpa34, pREP41-Sp-Rpa34, pRS425-P_{PGK}-Rpa49 (2μ-RPA49), pGID-Rpa49, pFL36-Rpa34, pRS425-pEB5-Rpa34 (YFP-Rpa34), pGID-Rpa34, pRS425-P_{PGK}-Rpa34DC58 (Rpa34-ΔC), and pEB5-Rpa34DC58 (YFP-Rpa34ΔC) were obtained by LR reaction between destination vectors and entry vector and named according to vectors used. Plasmids pGEX-6P-3, pGEX-6P-3-rpa49GST, pet28a-rpa43HA, and pet28a-rpa34HA were used for recombinant expression in *E. coli* and are described for expression.

Complementation was tested using plasmid-shuffling assays. A null allele of haploid tester strain is complemented by the corresponding WT genes borne on *URA3*-containing plasmids. Fluoroorotate (FOA) is toxic for *URA3+* strains (Boeke et al., 1984). FOA is used to apply a strong positive selection on cells without plasmids containing WT genes. Complementation is tested by examining whether plasmids expressing a given cDNA could bypass the lethal phenotype, monitored by FOA colonies.

GIM

GIM analysis of *RPA34* deletion mutant was performed as described previously (Decourty et al., 2008). Microarray data were normalized using MATLAB (MathWorks, Inc.), and relative enrichments are described in Table S3. Genetic interactions of interest were individually confirmed by plasmid-shuffling experiments. Deletion mutants of interest from the EUROSCARF collection were mated individually with the query strain carrying *RPA34* deletion tag with *NAT* marker under the control of the

MF(ALPHA)2/YGL089C promoter (prMFα2) that allowed selectivity for *MAT*α haploid cells (Decourty et al., 2008). The strain also contains the complementing plasmid pGID-RPA34 that allows expression of Rpa34 under the control of its own promoter terminator and carrying *HPH* and *klURA3* markers. Diploids were selected on YPD medium complemented with hygromycin and G418. Double mutants were generated by sporulation of diploids on RSS media and selection on YPD complemented with hygromycin, G418, and ClonNat.

Immunoprecipitation, sucrose gradient, antibodies, and pulse-field gel electrophoresis (PFGE)

Immunoprecipitation of Rpa190 with coexpressed CAST and PAF53 was performed as described previously (Galy et al., 2004). In brief, yeast cells were lysed by French press in buffer A (10 mM Hepes, pH 7.5, 150 mM KCl, 1.5 mM MgCl$_2$, 1 mM DTT, 1 mM PMSF, 0.1% Triton X-100, 10 µg/ml leupeptin, and 10 µg/ml pepstatin). The lysates were centrifuged at 15,000 *g* for 30 min at 4°C. TAP-tagged Rpa190 was purified using IgG Sepharose, and bound fractions were eluted with acid elution. Isolation of ribosomes under low salt conditions by sucrose gradient centrifugation was performed as previously described (Gadal et al., 2002). In summary, cells were harvested and lysed by vortexing with glass beads in buffer containing 10 mM Tris-HCl, pH 7.5, 100 mM NaCl, 30 mM MgCl$_2$, and 0.35 mM cycloheximid. Nuclei and cell debris were pelleted by centrifugation at 14,000 *g* for 5 min at 4°C. Ribosomal subunits were separated by centrifugation for 12 h at 100,000 *g* in a SW40 rotor at 4°C on a 10–40% sucrose gradient prepared in the lysis buffer. Immunoprecipitation of Pol I dimers from diploid yeast strain bearing Rpa190-HA and Rpa190-Myc (BEN24) was derived from chromatin immunoprecipitation procedures. Exponentially growing cells were treated with formaldehyde 1% final concentration during 15 min. Cell were lysed using glass beads in Precellys24 (Precellys). Soluble material was discarded, and chromatin pellet was recovered after 3,500 *g* centrifugation for 5 min. Chromatin was resuspended, sheared using sonication, then treated with 20 U RQ1 DNase (Promega) for 100 µl of extract for 30 min at 37°C. Pol I Immunoprecipitation from such chromatin fraction was performed as described previously (Galy et al., 2004). Antibodies used were anti-HA (12CA5; Babco), anti-Myc (9E10.3; Santa Cruz Biotechnology, Inc.), anti-PAF53 (P95220; BD), and anti-Nhp2 (Henras et al., 2001). The monoclonal antibody 72B9 (provided by J. Cavaillé, University of Toulouse, Toulouse, France) was produced and characterized as an anti-fibrillarin antibody cross-reacting with the budding yeast Nop1 (Reimer et al., 1987). PFGE was performed using CHEF-DRIII (Bio-Rad Laboratories). Budding yeast chromosomes were separated in a 1% agarose gel using a 87–162 switch time ramp at an included angle of 120° during 24 h at 6 V/cm. Southern hybridization was performed using a 3.5-kb NcoI–NcoI fragment from pNOY373 (Wai et al., 2000) as an rDNA probe, labeled by random priming (Megaprime DNA labeling system; GE Healthcare).

Expression of GST-Rpa49 and Rpa43 and Rpa34 in *E. coli*

Genes encoding Rpa43 and Rpa34 were cloned into the pET28a vector, harboring the kanamycin-resistance marker. These genes were amplified from genomic DNA with the primers 804–805 and 806–807, respectively, adding a C-terminal tag HA before inserting them into pET-28a (EMD) at site NcoI–BamHI. pGEX-6P-3 (GE Healthcare) harboring the ampicillin-resistance marker was used for GST expression. The Rpa49 gene was cloned into the pGEX-6P-3 vector, harboring the ampicillin-resistance marker and allowing N-terminal tagging with GST. For coexpression, the *E. coli* BL21 (Agilent Technologies) was transformed with (a) pGEX-6P-3-rpa49GST plus pet28α-rpa43HA, (b) pGEX-6P-3-rpa49GST plus pet28α-rpa34HA, (c) pGEX-6P-3 plus pet28α-rpa43HA, or (d) pGEX-6P-3 plus pet28α-rpa34HA. Transformed strains were inoculated in 0.2 liters of minimal medium plus ampicillin kanamycin with 0.01 overnight culture and grown to an OD$_{600}$ of 0.6 at 37°C, and production of recombinant proteins was induced for 3 h at 37°C with 0.1 mM isopropyl-D-thiogalactopyranoside. Purification of GST-tagged proteins was performed as described previously (Künzler and Hurt, 1998). The *E. coli* cell pellet was resuspended in 1% PBS buffer Triton X-100, and cells were lysed by sonication. The supernatant was incubated with 100 µl glutathione Sepharose 4B (Amersham), the beads were washed with lysis buffer, and the proteins bound to the beads were eluted with sample buffer. GST and GST-Rpa49 expression were confirmed by SDS-PAGE followed by Coomassie staining. Detection of Rpa43-HA and Rpa34-HA was achieved by Western blotting using HA peroxydase (Roche).

Fluorescent microscopy

After centrifugation, yeast cells were resuspended in synthetic complete medium (DIFCO), mounted on a slide, and observed in the fluorescence microscope. Wide-field fluorescent images were captured with a microscope (IX-81; Olympus) equipped with a polychrome V monochromator and a camera (CoolSNAP HQ; Roper Industries) controlled with Meta-Morph acquisition software (version 6; Universal Imaging Corp.). Confocal microscopy was performed using a Nipkow-disk confocal system (Revolution; Andor) installed on a microscope (IX-81), featuring a confocal spinning disk unit (CSU22; Yokogawa) and a cooled electron multiplying charge-coupled device camera (DU 888; Andor). The system was controlled using the FAST mode of Revolution IQ software (Andor). Images were acquired using a 100× Plan Apo 1.4 NA oil immersion objective and a twofold lens in the optical path. Single laser lines used for excitation were diode-pumped solid-state lasers exciting GFP fluorescence at 488 nm (50 mW; Coherent) and mCherry fluorescence at 561 nm (50 mW; Cobolt jive), and a bi-bandpass emission filter (Em01-R488/568-15; Semrock) allowed collection of the green and red fluorescence. Pixel size was 65 nm. For quantification of nucleolar volume, z stacks of 41 images with a 250-nm z step were used. Exposure time was 200 ms. Digital pictures were processed using Photoshop software (version CS3; Adobe).

Electron microscopy and quantitative analysis of Miller spreads

For morphological analysis of nucleoli, budding yeast were cryofixed by high pressure freezing (EMPACT; Leica) and cryosubstituted with 0.02% OsO$_4$, 0.1% uranyl acetate, and 1% glutamate in acetone for 72 h. Cells were embedded in a Lowicryl resin (HM-20) polymerized at −50°C. Sections of 100 nm were analyzed with a 1,200× electron microscope (Jeol).

Chromatin spreading was performed as described previously with minor modifications (Osheim et al., 2009). Carbon-coated grids were made hydrophilic by glow discharge instead of ethanol treatment. Depending on the contrast of the spread chromatin, counterstaining with heavy metal can be avoided. Negatively stained chromatin was obtained by short incubation with heavy metal followed by quick drying of the sample. The positions of polymerases and rDNA fiber were determined by visual inspection of micrographs using ImageJ (National Institutes of Health). Digital pictures were processed using Photoshop.

Simulated distances and 3D modeling

We estimated experimental measurement errors of 2 pixels of systematic bias and 2 pixels of random error, with a pixel size of 3 nm. Random and simulated distances between adjacent polymerases were determined assuming 185 possible Pol I positions on a single rDNA gene (12 nm for each polymerase distributed along a 2.22-µm-long gene). Measurement error was added to each distance, random noise being approximated using the normal law of 5 nm of variance. Each random and simulated dataset corresponds to 100 genes with 142, 62, or 36 polymerases per gene for 25 copy, 190 copy WT, and 25 copy strains bearing *rpa49Δ*, respectively. Distances were generated using MATLAB. Fitting of atomic coordinates into electron microscopy density maps, modeling of two successive elongating Pol I molecules, and image creation were performed using University of California San Francisco chimera (Pettersen et al., 2004).

Online supplemental material

Table S1 lists yeast strains used in this study. Table S2 lists oligonucleotides used in this study. GIM analysis of *RPA34* deletion mutant was performed as described previously (Decourty et al., 2008). Online supplemental material is available at http://www.jcb.org/cgi/content/full/jcb.201006040/DC1.

References

Basi, G., E. Schmid, and K. Maundrell. 1993. TATA box mutations in the *Schizosaccharomyces pombe* nmt1 promoter affect transcription efficiency but not the transcription start point or thiamine repressibility. *Gene.* 123:131–136. doi:10.1016/0378-1119(93)90552-E

Beckouet, F., S. Labarre-Mariotte, B. Albert, Y. Imazawa, M. Werner, O. Gadal, Y. Nogi, and P. Thuriaux. 2008. Two RNA polymerase I subunits control the binding and release of Rrn3 during transcription. *Mol. Cell. Biol.* 28:1596–1605. doi:10.1128/MCB.01464-07

Berger, A.B., L. Decourty, G. Badis, U. Nehrbass, A. Jacquier, and O. Gadal. 2007. Hmo1 is required for TOR-dependent regulation of ribosomal protein gene transcription. *Mol. Cell. Biol.* 27:8015–8026. doi:10.1128/MCB.01102-07

Berger, A.B., G.G. Cabal, E. Fabre, T. Duong, H. Buc, U. Nehrbass, J.C. Olivo-Marin, O. Gadal, and C. Zimmer. 2008. High-resolution statistical mapping reveals gene territories in live yeast. *Nat. Methods.* 5:1031–1037. doi:10.1038/nmeth.1266

Bischler, N., L. Brino, C. Carles, M. Riva, H. Tschochner, V. Mallouh, and P. Schultz. 2002. Localization of the yeast RNA polymerase I-specific subunits. *EMBO J.* 21:4136–4144. doi:10.1093/emboj/cdf392

Boeke, J.D., F. LaCroute, and G.R. Fink. 1984. A positive selection for mutants lacking orotidine-5′-phosphate decarboxylase activity in yeast: 5-fluoro-orotic acid resistance. *Mol. Gen. Genet.* 197:345–346. doi:10.1007/BF00330984

Bon, M., S.J. McGowan, and P.R. Cook. 2006. Many expressed genes in bacteria and yeast are transcribed only once per cell cycle. *FASEB J.* 20:1721–1723. doi:10.1096/fj.06-6087fje

Cioci, F., L. Vu, K. Eliason, M. Oakes, I.N. Siddiqi, and M. Nomura. 2003. Silencing in yeast rDNA chromatin: reciprocal relationship in gene expression between RNA polymerase I and II. *Mol. Cell.* 12:135–145. doi:10.1016/S1097-2765(03)00262-4

Cramer, P., K.J. Armache, S. Baumli, S. Benkert, F. Brueckner, C. Buchen, G.E. Damsma, S. Dengl, S.R. Geiger, A.J. Jasiak, et al. 2008. Structure of eukaryotic RNA polymerases. *Annu. Rev. Biophys.* 37:337–352. doi:10.1146/annurev.biophys.37.032807.130008

De Carlo, S., C. Carles, M. Riva, and P. Schultz. 2003. Cryo-negative staining reveals conformational flexibility within yeast RNA polymerase I. *J. Mol. Biol.* 329:891–902. doi:10.1016/S0022-2836(03)00510-2

Decourty, L., C. Saveanu, K. Zemam, F. Hantraye, E. Frachon, J.C. Rousselle, M. Fromont-Racine, and A. Jacquier. 2008. Linking functionally related genes by sensitive and quantitative characterization of genetic interaction profiles. *Proc. Natl. Acad. Sci. USA.* 105:5821–5826. doi:10.1073/pnas.0710533105

French, S.L., Y.N. Osheim, F. Cioci, M. Nomura, and A.L. Beyer. 2003. In exponentially growing *Saccharomyces cerevisiae* cells, rRNA synthesis is determined by the summed RNA polymerase I loading rate rather than by the number of active genes. *Mol. Cell. Biol.* 23:1558–1568. doi:10.1128/MCB.23.5.1558-1568.2003

Gadal, O., S. Mariotte-Labarre, S. Chédin, E. Quemeneur, C. Carles, A. Sentenac, and P. Thuriaux. 1997. A34.5, a nonessential component of yeast RNA polymerase I, cooperates with subunit A14 and DNA topoisomerase I to produce a functional rRNA synthesis machine. *Mol. Cell. Biol.* 17:1787–1795.

Gadal, O., D. Strauss, E. Petfalski, P.E. Gleizes, N. Gas, D. Tollervey, and E. Hurt. 2002. Rlp7p is associated with 60S preribosomes, restricted to the granular component of the nucleolus, and required for pre-rRNA processing. *J. Cell Biol.* 157:941–951. doi:10.1083/jcb.200111039

Galy, V., O. Gadal, M. Fromont-Racine, A. Romano, A. Jacquier, and U. Nehrbass. 2004. Nuclear retention of unspliced mRNAs in yeast is mediated by perinuclear Mlp1. *Cell.* 116:63–73. doi:10.1016/S0092-8674(03)01026-2

Geiger, S.R., K. Lorenzen, A. Schreieck, P. Hanecker, D. Kostrewa, A.J. Heck, and P. Cramer. 2010. RNA polymerase I contains a TFIIF-related DNA-binding subcomplex. *Mol. Cell.* 39:583–594. doi:10.1016/j.molcel.2010.07.028

Hanada, K., C.Z. Song, K. Yamamoto, K. Yano, Y. Maeda, K. Yamaguchi, and M. Muramatsu. 1996. RNA polymerase I associated factor 53 binds to the nucleolar transcription factor UBF and functions in specific rDNA transcription. *EMBO J.* 15:2217–2226.

Henras, A., C. Dez, J. Noaillac-Depeyre, Y. Henry, and M. Caizergues-Ferrer. 2001. Accumulation of H/ACA snoRNPs depends on the integrity of the conserved central domain of the RNA-binding protein Nhp2p. *Nucleic Acids Res.* 29:2733–2746. doi:10.1093/nar/29.13.2733

Hernandez-Verdun, D., P. Roussel, and J. Gébrane-Younès. 2002. Emerging concepts of nucleolar assembly. *J. Cell Sci.* 115:2265–2270.

Huet, J., J.M. Buhler, A. Sentenac, and P. Fromageot. 1975. Dissociation of two polypeptide chains from yeast RNA polymerase A. *Proc. Natl. Acad. Sci. USA.* 72:3034–3038. doi:10.1073/pnas.72.8.3034

Kuhn, C.D., S.R. Geiger, S. Baumli, M. Gartmann, J. Gerber, S. Jennebach, T. Mielke, H. Tschochner, R. Beckmann, and P. Cramer. 2007. Functional architecture of RNA polymerase I. *Cell.* 131:1260–1272. doi:10.1016/j.cell.2007.10.051

Künzler, M., and E.C. Hurt. 1998. Cse1p functions as the nuclear export receptor for importin alpha in yeast. *FEBS Lett.* 433:185–190. doi:10.1016/S0014-5793(98)00892-8

Kwapisz, M., F. Beckouët, and P. Thuriaux. 2008. Early evolution of eukaryotic DNA-dependent RNA polymerases. *Trends Genet.* 24:211–215. doi:10.1016/j.tig.2008.02.002

Lechertier, T., V. Sirri, D. Hernandez-Verdun, and P. Roussel. 2007. A B23-interacting sequence as a tool to visualize protein interactions in a cellular context. *J. Cell Sci.* 120:265–275. doi:10.1242/jcs.03345

Liljelund, P., S. Mariotte, J.M. Buhler, and A. Sentenac. 1992. Characterization and mutagenesis of the gene encoding the A49 subunit of RNA polymerase A in *Saccharomyces cerevisiae*. *Proc. Natl. Acad. Sci. USA.* 89:9302–9305. doi:10.1073/pnas.89.19.9302

Miller, O.L. Jr., and B.R. Beatty. 1969. Visualization of nucleolar genes. *Science.* 164:955–957. doi:10.1126/science.164.3882.955

Minakhin, L., S. Bhagat, A. Brunning, E.A. Campbell, S.A. Darst, R.H. Ebright, and K. Severinov. 2001. Bacterial RNA polymerase subunit omega and eukaryotic RNA polymerase subunit RPB6 are sequence, structural, and functional homologs and promote RNA polymerase assembly. *Proc. Natl. Acad. Sci. USA.* 98:892–897. doi:10.1073/pnas.98.3.892

Misteli, T. 2001. The concept of self-organization in cellular architecture. *J. Cell Biol.* 155:181–185. doi:10.1083/jcb.200108110

Nakagawa, K., K. Hisatake, Y. Imazawa, A. Ishiguro, M. Matsumoto, L. Pape, A. Ishihama, and Y. Nogi. 2003. The fission yeast RPA51 is a functional homolog of the budding yeast A49 subunit of RNA polymerase I and required for maximizing transcription of ribosomal DNA. *Genes Genet. Syst.* 78:199–209. doi:10.1266/ggs.78.199

Nogi, Y., R. Yano, and M. Nomura. 1991. Synthesis of large rRNAs by RNA polymerase II in mutants of *Saccharomyces cerevisiae* defective in RNA polymerase I. *Proc. Natl. Acad. Sci. USA.* 88:3962–3966. doi:10.1073/pnas.88.9.3962

Oakes, M., J.P. Aris, J.S. Brockenbrough, H. Wai, L. Vu, and M. Nomura. 1998. Mutational analysis of the structure and localization of the nucleolus in the yeast *Saccharomyces cerevisiae*. *J. Cell Biol.* 143:23–34. doi:10.1083/jcb.143.1.23

Osheim, Y.N., S.L. French, M.L. Sikes, and A.L. Beyer. 2009. Electron microscope visualization of RNA transcription and processing in *Saccharomyces cerevisiae* by Miller chromatin spreading. *Methods Mol. Biol.* 464:55–69. doi:10.1007/978-1-60327-461-6_4

Panov, K.I., T.B. Panova, O. Gadal, K. Nishiyama, T. Saito, J. Russell, and J.C. Zomerdijk. 2006. RNA polymerase I-specific subunit CAST/hPAF49 has a role in the activation of transcription by upstream binding factor. *Mol. Cell. Biol.* 26:5436–5448. doi:10.1128/MCB.00230-06

Pettersen, E.F., T.D. Goddard, C.C. Huang, G.S. Couch, D.M. Greenblatt, E.C. Meng, and T.E. Ferrin. 2004. UCSF Chimera—a visualization system for exploratory research and analysis. *J. Comput. Chem.* 25:1605–1612. doi:10.1002/jcc.20084

Reimer, G., I. Raska, E.M. Tan, and U. Scheer. 1987. Human autoantibodies: probes for nucleolus structure and function. *Virchows. Arch. B Cell Pathol. Incl. Mol. Pathol.* 54:131–143. doi:10.1007/BF02899205

Rigaut, G., A. Shevchenko, B. Rutz, M. Wilm, M. Mann, and B. Séraphin. 1999. A generic protein purification method for protein complex characterization and proteome exploration. *Nat. Biotechnol.* 17:1030–1032. doi:10.1038/13732

Samkurashvili, I., and D.S. Luse. 1998. Structural changes in the RNA polymerase II transcription complex during transition from initiation to elongation. *Mol. Cell. Biol.* 18:5343–5354.

Schneider, D.A., A. Michel, M.L. Sikes, L. Vu, J.A. Dodd, S. Salgia, Y.N. Osheim, A.L. Beyer, and M. Nomura. 2007. Transcription elongation by RNA polymerase I is linked to efficient rRNA processing and ribosome assembly. *Mol. Cell.* 26:217–229. doi:10.1016/j.molcel.2007.04.007

Sikorski, R.S., and P. Hieter. 1989. A system of shuttle vectors and yeast host strains designed for efficient manipulation of DNA in *Saccharomyces cerevisiae*. *Genetics.* 122:19–27.

Trumtel, S., I. Léger-Silvestre, P.E. Gleizes, F. Teulières, and N. Gas. 2000. Assembly and functional organization of the nucleolus: ultrastructural analysis of *Saccharomyces cerevisiae* mutants. *Mol. Biol. Cell.* 11:2175–2189.

Van Mullem, V., M. Wery, X. De Bolle, and J. Vandenhaute. 2003. Construction of a set of *Saccharomyces cerevisiae* vectors designed for recombinational cloning. *Yeast.* 20:739–746. doi:10.1002/yea.999

Wai, H.H., L. Vu, M. Oakes, and M. Nomura. 2000. Complete deletion of yeast chromosomal rDNA repeats and integration of a new rDNA repeat: use of rDNA deletion strains for functional analysis of rDNA promoter elements in vivo. *Nucleic Acids Res.* 28:3524–3534. doi:10.1093/nar/28.18.3524

Wang, D., D.A. Bushnell, K.D. Westover, C.D. Kaplan, and R.D. Kornberg. 2006. Structural basis of transcription: role of the trigger loop in substrate specificity and catalysis. *Cell.* 127:941–954. doi:10.1016/j.cell.2006.11.023

Yamamoto, K., M. Yamamoto, K. Hanada, Y. Nogi, T. Matsuyama, and M. Muramatsu. 2004. Multiple protein-protein interactions by RNA polymerase I-associated factor PAF49 and role of PAF49 in rRNA transcription. *Mol. Cell. Biol.* 24:6338–6349. doi:10.1128/MCB.24.14.6338-6349.2004

Yamazaki, T., Y. Hamano, H. Tashiro, K. Itoh, H. Nakano, S. Miyatake, and T. Saito. 1999. CAST, a novel CD3epsilon-binding protein transducing activation signal for interleukin-2 production in T cells. *J. Biol. Chem.* 274:18173–18180. doi:10.1074/jbc.274.26.18173